Article

The International Journal of
Robotics Research
1–13

DOI: 10.1177/0278364915584806
ijr.sagepub.com

Hybrid motion/force control of multi-backbone continuum robots

Andrea Bajo and Nabil Simaan

Abstract

The recent growth of surgical applications exploiting continuum robots demands for new control paradigms that ensure safety by controlling interaction forces of tele-operated end-effectors. In this paper, we present the modeling, sensing and control of multi-backbone continuum robots in a unified framework for hybrid motion/force control. Multi-backbone continuum robots allow to estimate forces and torques at the operational point by monitoring loads along their actuation lines without the need for a dedicated transducer at the operational point. This capability is indeed crucial in emerging fields such as robotic surgery where cost and strict sterilization guidelines prevent the adoption of a dedicated sensor to provide force feedback from the sterile field. To advance further the force sensing capabilities of multi-backbone continuum robots, we present a new framework for hybrid motion and force control of continuum robots with intrinsic force sensing capabilities. The framework is based on a kinetostatic modeling of the multi-backbone continuum robot with, a simplified model for online estimate of the manipulator's compliance, and a new strategy for merging force and motion control laws in the configuration space of the manipulator. Experimental results show the ability to sense and regulate forces at the operational point and evaluate the framework for shape exploration and stiffness imaging in flexible environments.

Keywords

Force control, continuum robots

1. Introduction

Successful and safe interaction with the environment requires robotic manipulators to control motions and forces at their operational point while complying with contact and motion constraints (Khatib, 1987). When contact between the robot's end-effector and a rigid environment occurs, reaction forces prevent motions in normal directions while allowing translation of the contact point in the tangential directions. These directions vary depending on contact and friction between the two bodies (Mason and Salisbury, 1985).

There are mainly two methodologies to control interaction forces and motions, *impedance control* (Hogan, 1985) and *hybrid motion/force control* (Raibert and Craig, 1981). Impedance control, a generalization of *admittance control* (Whitney, 1977) and *stiffness control* (Salisbury, 1980), aims at regulating the mechanical impedance of the operational point in contact with a rigid environment. As a consequence, directions in which position should be controlled accurately are assigned large impedance, while directions in which the end-effector should comply with the environment are assigned a small impedance. On the other hand, hybrid motion/force control decouples control signals produced by two independent motion and force controllers by projecting their control signals into orthogonal directions in which motions and forces should be independently controlled.

The main difference between the two methodologies is that impedance control indirectly regulates force via a position feedback, while hybrid motion/force control exploits both position and force loops. The advantage of impedance control is that mode switching at the time of contact and accurate a priori knowledge of the geometric constraint and elasticity of the environment are not necessary. On the other hand, hybrid motion/force control requires a fairly accurate knowledge of the contact constraint and may produce unstable behaviors during the impact phase because of the intermittent switching in control modes. However, when the robotic manipulator is required to accurately control position and force, the hybrid motion/force control provides superior results. For the interested reader, an exhaustive

Advanced Robotics and Mechanism Applications (ARMA), Department of Mechanical Engineering, Vanderbilt University, Nashville, TN, USA

Corresponding author:
Andrea Bajo, 2616 Erwin Road, Durham, NC 27705, USA.
Email: andrea.bajo@gmail.com

overview of these two methods, variants and applications are described in Yoshikawa (2000).

Continuum robots are continuously bending, compliant, infinite-degree-of-freedom structures (Robinson and Davies, 1999; Webster III and Jones, 2010) that have gained steadily increasing attention by both the robotics and medical communities. The innate compliance of these devices makes them strong candidates for medical applications such as minimally invasive surgery (Simaan et al., 2009), cardio-thoracic therapy (Camarillo et al., 2008), neuro-surgery (Mahvash and Dupont, 2010) and unstructured tasks such as the grasping of unknown objects (Jones and Walker, 2006). However, passive compliance comes with a price of performance degradation in terms of position accuracy, payload and force exchange capabilities.

Modeling of continuum robots builds upon the early work on hyper-redundant manipulators where high-degree-of-freedom structures were modeled using a modal representation of backbone curves (Chirikjian and Burdick, 1994), splines (Zanganeh and Angeles, 1995) and a set of differential equations (Chirikjian, 1993) minimizing the strain energy along the backbone curve. The kinematics of single- and multi-segment continuum robots was initially presented as a series of natural basis functions (Gravagne and Walker, 2000) and evaluated with bending and prismatic segments (Hannan and Walker, 2003). In an effort to reduce the computational burden of these methods, researchers focused on algorithms for real-time implementation (Jones and Walker, 2006) and closed-form solutions based on the assumption of constant-curvature for tendon-driven (Camarillo et al., 2008) and multi-backbone push-pull segments (Xu and Simaan, 2010a).

Motion control of continuum robots is generally carried out with a combination of three compensation strategies: model-based, adaptive and close-loop. Model-based compensation includes friction modeling (Kesner et al., 2011), back-lash identification and correction (Agrawal et al., 2010), extension of actuation lines (Xu and Simaan, 2006) and kinematic coupling between serially-stacked segments (Simaan et al., 2009). Adaptive control strategies that augment the model-based actuation compensation have also been proposed using nonlinear observers (Ivanescu and Stoian, 1995), sliding-mode controllers (Piltan and Tayebi Haghighi, 2012), neural networks (Braganza et al., 2007) and modeling of large deflection dynamics (Gravagne et al., 2003). Finally, closed-loop control strategies include a variegated use of sensors and multiple loops closed at different levels of the control framework. For example, researchers have investigated single-camera vision algorithms (Croom et al., 2010), multi-camera vision methods (Camarillo et al., 2009), string pots and encoders (Trivedi and Rahn, 2014) and electro-magnetic trackers (Penning et al., 2011) to provide information about the current configuration of the continuum manipulator. In an effort to enhance further the control performance, scholars have proposed mixed feedback controllers that uses both a joint-space control loop and a configuration-space control loop (Bajo et al., 2011), task-space closed-loop control (Penning et al., 2011) and versatile controllers that are applicable both to configuration-space and task-space control (Kapadia et al., 2014).

As continuum robots are deployed in increasingly delicate tasks and environments, researchers have recently began investigating algorithms for stiffness control, compliant motion control and indirect force control. In Mahvash and Dupont (2011), the authors proposed a method for combining the nominal forward kinematics and the deflection of the manipulator due to the external load to generate the desired tip stiffness. In Goldman et al. (2014), the authors proposed a method that allows a multi-backbone continuum robot to autonomously comply to interaction forces acting at unknown locations. In Kesner and Howe (2011), the authors proposed an indirect force controller for flexible tendon-driven catheters. To the best of the authors' knowledge, there are no algorithms for direct force control and hybrid/motion control of continuum robots. This gap is mainly due to a lack of sensorial technology able to miniaturize force sensors and the formulation of a general framework that applies to flexible manipulators.

In an effort to provide miniature robotic manipulators with force feedback, researchers mainly investigated two methodologies: 1) design and manufacturing of miniature sensors for minimally invasive surgery (Baki et al., 2012; Seibold et al., 2005; Valdastri et al., 2006); 2) algorithms for *intrinsic force sensing* (Rucker and Webster III, 2011; Wei and Simaan, 2012; Xu and Simaan, 2010b) Although the first methodology provides a direct measure of the force at the tip, its wide use is limited by cost, robustness, the increasing demand of magnetic resonance imaging (MRI) compatible surgical instruments, sterilizability and miniaturization. On the other hand, the second methodology views the entire robot as both a multi-axis force sensor and a dexterous end-effector. The advantage of this approach is that sensors are placed away from the surgical site reducing the burden of providing sterilizable instruments.

This paper complements previous works aimed at providing multi-backbone continuum robots with a set of modeling, estimation and control algorithms for full characterization of their interaction with the environment. Full characterization of the interaction includes: discerning collisions, localizing contacts, estimating interaction forces and autonomously complying with the environment at any point along their flexible spine. In Xu and Simaan (2008, 2010b), a method for the estimation of wrenches at the tip of a single- and multi-segment continuum robot was proposed and validated. In Bajo and Simaan (2010, 2012), the authors proposed the problem of contact detectably and multiple algorithms for detection and localization of contacts along multi-segment continuum robots. In Goldman

et al. (2014), an algorithm for compliant motion control of continuum robots without a priori knowledge of interaction points was presented. In Tully et al. (2012), the use of contact detection and a constrained Kalman filter to register a flexible robot to a flexible environment was demonstrated. In Sanan et al. (2014), we extended this framework to use force controlled scans of a flexible environment based on the algorithm described in this work, to register shape and stiffness maps of the environment to pre-operative models.

The contribution of this work is a complete framework for hybrid motion/force control of continuum robots with force sensing capabilities. The force feedback can be provided by either a dedicated multi-axis force sensor at the tip or one of the intrinsic force sensing methods proposed in the literature. The force and position control signals are merged in the configuration space of the continuum manipulator via two transformations. The first transformation computes the desired configuration space velocities that achieve the desired task space velocities via the inverse Jacobian matrix. The second transformation computes the desired configuration space velocities that achieve the desired task space forces via the compliance matrix of the flexible manipulator. The joint-space control input is then computed using the inverse position solution and a model-based actuation compensation method. The actuation compensation method has a twofold contribution: it compensates for actuation line extensions and provides a feed-forward term for the desired task space force to be applied at the tip of the manipulator. The hybrid motion/force control framework for continuum robots is evaluated on a multi-backbone continuum robot with intrinsic force sensing that is suitable for minimally invasive surgery and natural orifice translumenal endoscopic surgery.

2. Assumptions

In this section, we outline the assumptions made in the remainder of this work. First, we assume that the kinematic model of the flexible manipulator is known and that the robot is equipped with means for measuring or estimating environmental interaction forces. This information would be provided by intrinsic wrench estimation (Xu and Simaan, 2008) or by a dedicated miniature multi-axis force sensor placed at the operational point if the application domain allows for use of such a sensor. In this work, a multi-backbone continuum robot with intrinsic wrench estimation capabilities is used to evaluate the hybrid motion/force control framework. The following assumptions specifically apply to multi-backbone continuum robots with intrinsic force sensing.

1. The continuum robot segments bend in circular shapes and gravitational forces are negligible. This assumption was verified in Xu and Simaan (2008, 2010a) for small robots such as the one used in this work.
2. The continuum robot is able to sense actuation forces via load cells placed between each actuation line and its actuator. Examples of actuation units with force sensing capabilities are provided in Xu and Simaan (2008) and in Goldman et al. (2013).
3. The geometric constraint is known and the environment is rigid. This information is used for both the hybrid motion/force controller and the intrinsic wrench estimation. However, because of the innate compliance of continuum robots as demonstrated by experimental results, an exact knowledge of the geometric constraint is not necessary.
4. The only interaction point between the continuum robot and the environment is at the operational point.
5. An approximate model of the compliance matrix of the continuum manipulator is available, the force control-loop rate is adequate and the interaction force at the operational point of the robot is not sufficiently large to cause large deformations of the continuum structure. This assumption was verified in Goldman et al. (2014).

3. Modeling of the multi-backbone continuum robot

Figure 1 shows a one segment multi-backbone continuum robot mounted on a linear stage capable of controlling insertion depth $\mathbf{q}_{ins}$ along the $\hat{\mathbf{z}}_0$-axis of the world frame. The segment has three *push-pull* backbones that allows for bending its end disk in space. A complete derivation of the direct and differential kinematics of these continuum structures are given in Xu and Simaan (2008) and Simaan et al. (2009). For the ease of presentation, in the remainder of this section, the kinematics and statics of the manipulator are summarized. Six coordinate systems are defined: 1) world frame $\{\hat{\mathbf{x}}_0, \hat{\mathbf{y}}_0, \hat{\mathbf{z}}_0\}$; 2) base disk frame $\{\hat{\mathbf{x}}_1, \hat{\mathbf{y}}_1, \hat{\mathbf{z}}_1\}$; 3) bending plane frame $\{\hat{\mathbf{x}}_2, \hat{\mathbf{y}}_2, \hat{\mathbf{z}}_2\}$; 4) end-disk frame $\{\hat{\mathbf{x}}_3, \hat{\mathbf{y}}_3, \hat{\mathbf{z}}_3\}$; 5) gripper frame $\{\hat{\mathbf{x}}_4, \hat{\mathbf{y}}_4, \hat{\mathbf{z}}_4\}$; 6) probe frame $\{\hat{\mathbf{x}}_5, \hat{\mathbf{y}}_5, \hat{\mathbf{z}}_5\}$.

The position, $\mathbf{p}^0_{0,5}$, and the orientation, $\mathbf{R}^0_5$, of the probe frame $\{O_5\}$ are uniquely defined by configuration variables $\Psi = [\theta \quad \delta \quad q_{ins}]^T$. Angle θ is defined between vectors $\hat{\mathbf{z}}_5$ and $\hat{\mathbf{x}}_2$. Angle δ is defined about $\hat{\mathbf{z}}_1$ between vector $\hat{\mathbf{x}}_1$ and the bending plane. Finally, q_{ins} is the distance between frame $\{O_0\}$ and frame $\{O_1\}$. The pose of the end-effector is then given by

$$\mathbf{p}^0_{0,5} = \mathbf{p}^0_{0,1} + \mathbf{R}^0_2 \mathbf{p}^2_{2,3} + \mathbf{R}^0_4 \mathbf{p}^4_{4,5} \tag{1}$$

$$\mathbf{R}^0_5 = \mathbf{R}^0_1 \mathbf{R}^1_2 \mathbf{R}^2_3 \mathbf{R}^3_4 \mathbf{R}^4_5 \tag{2}$$

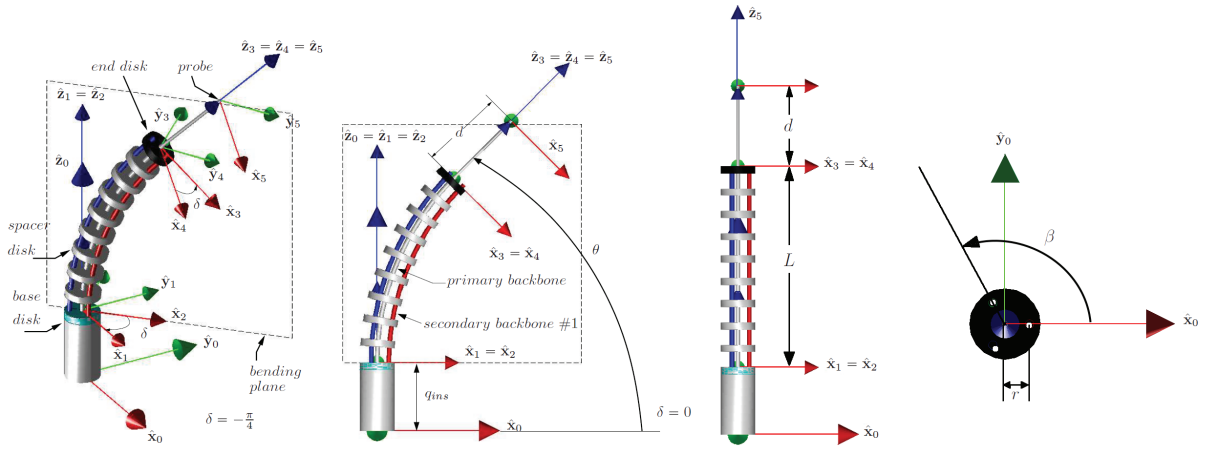

Fig. 1. Kinematics nomenclature used in this paper.

where $\mathbf{p}_{i,j}^{k}$ is the vector from the origin of frame $\{O_i\}$ to the origin of frame $\{O_j\}$ written in frame $\{O_k\}$ and matrix $\mathbf{R}_j^i$ represents the rotation from frame $\{O_j\}$ to frame $\{O_i\}$.

In order to achieve angles θ and δ, the secondary backbones of the continuum robot (i = 1, 2, 3) are shortened or lengthened as follows

$$q_i = r\cos(\delta_i)(\theta - \theta_0) \tag{3}$$

where $\delta_i = \delta + (i - 1)\beta$, $\beta = 2/3\pi$ and r is the radial distance of each secondary backbone from the centrally-located backbone. From equation (3), we define the augmented joint-space vector $\mathbf{q} \in \mathrm{IR}^4$ as

$$\mathbf{q} = [\, q_1 \quad q_2 \quad q_3 \quad q_{ins} \,]^T \tag{4}$$

The end-effector's twist, $\mathbf{t}$, is related to the rate of change of the configurations space variables, $\dot{\Psi}$, and the rate of change of the joint space variables, $\dot{\mathbf{q}}$, as

$$\mathbf{t} = \mathbf{J}_{t\psi}\dot{\Psi} \tag{5}$$

$$\dot{\mathbf{q}} = \mathbf{J}_{q\Psi}\dot{\Psi} \tag{6}$$

where $\mathbf{J}_{t\psi}$ is the geometric Jacobian relating configuration-space and task-space velocities and $\mathbf{J}_{q\Psi}$ is the Jacobian relating configuration-space and joint-space velocities.

Using virtual work arguments discussed in Simaan et al. (2009), the following first order linear relationship relates the actuation forces $\boldsymbol{\tau}$ to the configuration space vector $\boldsymbol{\Psi}$ and an external wrench $\mathbf{w}_e$ acting at the operational point

$$\mathbf{J}_{t\Psi}^T\mathbf{w}_e + \mathbf{J}_{q\Psi}^T\boldsymbol{\tau} = \nabla U \tag{7}$$

where U is the elastic energy stored by the continuum segment, and $\nabla U = \frac{\partial U}{\partial \Psi}$.

By defining $\mathbf{f}_\psi = \mathbf{J}_{t\Psi}^T\mathbf{W}_e$ as the *generalized force* vector, equation (7) yields

$$\mathbf{f}_\psi = \nabla U - \left[\mathbf{J}_{\mathbf{q}\psi}^{\mathrm{T}}\right]\boldsymbol{\tau} = \nabla U - \left[\mathbf{J}_{\mathbf{q}\psi}\right]^{\mathrm{T}}\boldsymbol{\tau} \tag{8}$$

For small perturbations from an equilibrium configuration, the stiffness of the continuum segment is described in configuration space as

$$\delta\mathbf{f}_\psi = \mathbf{K}_\psi\delta\boldsymbol{\psi} \tag{9}$$

where the stiffness is given by the Jacobian of the components of the generalized force associated with the continuum robot with respect to its configuration space perturbation as described in Goldman et al. (2014).

The robot's actuation lines stretch and compress due to their inherent flexibility. Therefore, actuation compensation methods need to be considered in order to achieve the desired configuration $\boldsymbol{\Psi}$ of the continuum segment. In Xu and Simaan (2006) and Simaan et al. (2009) several model-based estimation algorithms were presented in order to deal with actuation compensation of multi-backbone continuum robots. The compensation law is based on a compliance model of the actuation lines and the expected actuation forces $\boldsymbol{\tau}$ as obtained from equation (7). The expected stretch/compression on the actuation lines is obtained by

$$\varepsilon = \mathbf{C}_a\boldsymbol{\tau} \tag{10}$$

where the compliance matrix of the actuation lines $\mathbf{C}_a$ is given by

$$\mathbf{C}_a = \frac{L_{al}}{E_y A}\begin{bmatrix} \mathbf{I}_{3\times 3} & \mathbf{0} \\ \mathbf{0} & 0 \end{bmatrix} \tag{11}$$

and L_{al} is the length of the actuation lines, E_y is the Young's modulus of Nickel-Titanium (NiTi) and A is the cross-sectional area of the backbones. By accounting for the compliance model, the desired backbone displacement is then computed as

$$\widehat{\mathbf{q}}_{des} = \mathbf{q}_{des} + \varepsilon \tag{12}$$

where $\mathbf{q}_{des}$ are the desired joint values as defined in equation (4) based on a pure kinematic calculation and $\widehat{\mathbf{q}}_{des}$ also includes the actuation compensation law ε.

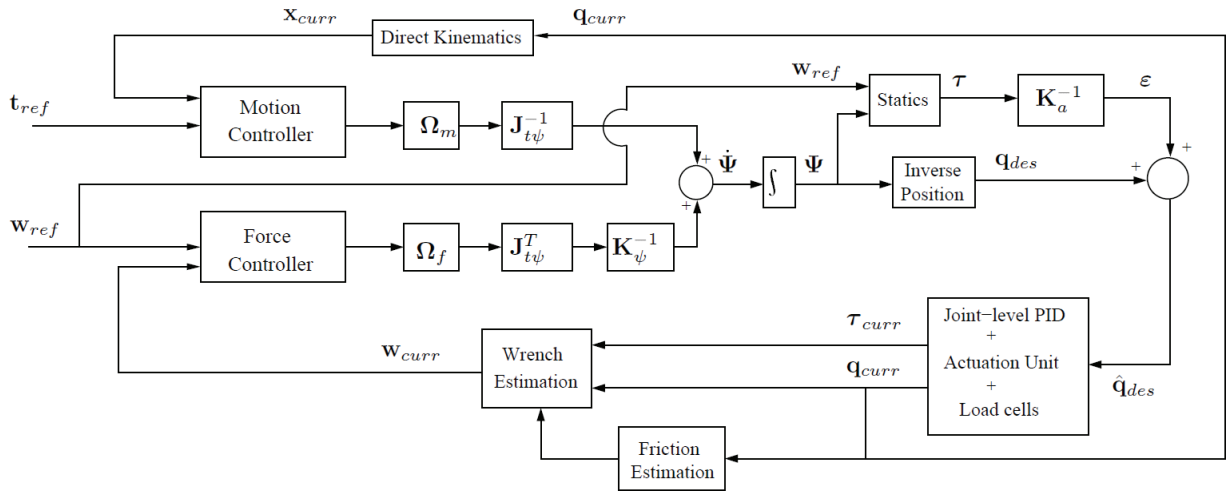

Fig. 2. Proposed hybrid motion/force control of multi-backbone continuum robots with intrinsic force sensing. $\mathbf{\Omega}_m$ and $\mathbf{\Omega}_f$ are projection matrices, $\mathbf{J}_{x\psi}$ is the Jacobian matrix, $\mathbf{K}_\psi$ is the configuration-space stiffness matrix, $\mathbf{\Psi}$ is the configuration space vector, $\mathbf{K}_a$ is the joint-space stiffness matrix.

4. Hybrid motion/force control for continuum robots

Figure 2 shows the proposed hybrid motion/force control architecture of multi-backbone continuum robots with intrinsic force sensing. As in the classic architecture proposed in Khatib (1987), two separate controllers produce motion and force commands that are transformed into allowable motion/force directions using projection matrices $\mathbf{\Omega}_m$ and $\mathbf{\Omega}_f$. The main difference in the proposed approach lies on the fact that the motion and force control commands are merged in *configuration space* of the continuum manipulator rather than in the actuator space as in the classic approach. In the reminder of this section, we provide justification and details of this control architecture starting with the task decomposition through the use of projection matrices.

4.1. Projection matrices

Hybrid motion/force control aims at controlling the force interaction by decoupling control inputs into allowable *relative motions* and *constraining wrenches*[1]. Regardless of the type of contact, two dual vector subspaces are defined (Featherstone, 2004; Lipkin and Duffy, 1988), one n-dimensional space of normal vectors $N \subseteq \mathrm{F}^6$ and one $(6\text{-}n)$-dimensional space of tangent vectors $T \subseteq \mathrm{M}^6$, where n is the degree of motion constraint. The bases of these two spaces are defined by a $6 \times n$ matrix $\mathbf{N}$ and a $6 \times (6 - n)$ matrix $\mathbf{T}$. The columns of $\mathbf{N}$ and $\mathbf{T}$ are respectively any n linearly independent wrench in N and any $6 - n$ linearly independent motion screws in T. As a consequence of the reciprocity condition and the contact constraint, the scalar product of any column of $\mathbf{N}$ with any column of $\mathbf{T}$ is zero. Although in many situations matrices $\mathbf{N}$ and $\mathbf{T}$ are simply the composition of canonical vectors in IR^6 and can be obtained by inspection (Mason, 1981), this is not the case when dealing with complex interaction tasks and multi-point contacts (Featherstone, 2004; Lipkin and Duffy, 1988).

The reciprocity of the control inputs is enforced by projecting each control input into the correct subspace by pre-multiplication of a projection matrix. We therefore define two projection matrices $\mathbf{\Omega}_f$ and $\mathbf{\Omega}_m$ that project any control input into consistent wrenches and twists respectively

$$\Omega_f = \mathbf{N}(\mathbf{N}^T\mathbf{N})^{-1}\mathbf{N}^T \tag{13}$$

$$\Omega_m = \mathbf{T}(\mathbf{T}^T\mathbf{T})^{-1}\mathbf{T}^T = \mathbf{I} - \Omega_f \tag{14}$$

It is worth noticing that equations (13) and (14) provide only two particular projection matrices. A general formulation that expresses general projections consistent with the given contact is discussed in Basilevsky (1983) and Featherstone (2004).

4.2. Configuration space projection

In the control of rigid-body robots, the dynamics of the manipulator is used to convert motion commands into actuator torque commands. Using this approach, the units of the output of the force and motion controllers are consistent (typically torques). This approach is not directly applicable to small continuum manipulators because these robots are inherently flexible, their masses very small and the dynamics of these robots is usually poorly characterized due to large friction and modeling uncertainties. Therefore, we propose to project control commands into the configuration space of the continuum robot. An estimate of the robot compliance allows to maintain the units consistency between the motion and the force controller branches.

The projection of the motion controller commands from task space to configuration space is achieved by multiplying

the twist by the inverse of the Jacobian matrix $\mathbf{J}_{t\psi}$ thus resulting in configuration space speeds $\dot{\boldsymbol{\Psi}}_m$. The projection of the force controller commands from task space to configuration space is achieved through the use of the transpose of the Jacobian matrix $\mathbf{J}_{t\psi}$ which results in generalized force $\mathbf{f}_{\psi}$. Using an estimate of the continuum robot compliance as presented in Goldman et al. (2014), $\mathbf{f}_{\psi}$ is then transformed into kinematically- and unit-consistent configuration space speeds $\dot{\boldsymbol{\Psi}}_f$ by pre-multiplying it with the configuration space compliance matrix $\mathbf{K}_{\Psi}^{-1}$. The commanded resultant configuration space speed is then given by

$$\dot{\boldsymbol{\Psi}} = \dot{\boldsymbol{\Psi}}_m + \dot{\boldsymbol{\Psi}}_{f_\psi} \tag{15}$$

Hence, the inverse position analysis of the continuum robot segment is used to calculate the theoretical desired joint-space positions $\mathbf{q}_{des}$. Using the intrinsic force sensing approach in Appendix A the wrench acting at the tip of the robot is estimated and substituted into equation (7). An additional joint-level actuation compensation term is then obtained using equation (10). This term includes both a compensation term for the applied wrench at the tip of the robot and a compensation term for extension and friction in the actuation lines.

4.3. Control architecture

The framework inputs are defined by the reference twist $\mathbf{t}_{ref} = \begin{bmatrix} \mathbf{v}_{ref}^T & \boldsymbol{\omega}_{ref}^T \end{bmatrix}^T$ and the reference interaction wrench at the operational point $\mathbf{w}_{ref} = \begin{bmatrix} \mathbf{f}_{ref}^T & \mathbf{m}_{ref}^T \end{bmatrix}^T$.

The reference end-effector twist and wrench are related to a desired twist $\mathbf{t}_{des}$ and a desired wrench $\mathbf{w}_{des}$ that are then used as inputs to low level motion and force controllers before conversion into configuration speed commands. Depending on the particular application, $\mathbf{t}_{des}$ may be equal to $\mathbf{t}_{ref}$ if speed is directly commanded by the user (e.g. direct speed telemanipulation control by the user) or $\mathbf{t}_{des}$ may be obtained directly from the end-effector position/orientation error using a resolved rates algorithm (e.g. Whitney (1969)). The desired wrench $\mathbf{w}_{des}$ is obtained using a proportional-integral force feedback control scheme such that

$$\mathbf{w}_{des} = \mathbf{K}_{f,p}\mathbf{w}_e + \mathbf{K}_{f,i}\int \mathbf{w}_e \tag{16}$$

where $\mathbf{K}_{f,p}$ and $\mathbf{K}_{f,i}$ are the proportional and integral feedback gains and $\mathbf{w}_e$ is the wrench error defined as

$$\mathbf{w}_e = \mathbf{w}_{ref} - \mathbf{w}_{curr} \tag{17}$$

and $\mathbf{w}_{ref}$, $\mathbf{w}_{curr}$ represent the reference and current estimated end-effector wrench, respectively.

The desired twist $\mathbf{t}_{des}$ and wrench $\mathbf{w}_{des}$ are then transformed into desired configuration speeds $\dot{\Psi}_m$ and $\dot{\boldsymbol{\Psi}}_{f_\psi}$ to reconcile the units of the motion and force controller outputs

$$\dot{\boldsymbol{\Psi}}_m = \mathbf{J}_{t\psi}{}^{\dagger}\Omega_m\mathbf{t}_{des} \tag{18}$$

$$\dot{\boldsymbol{\Psi}}_{f_\psi} = \mathbf{K}_{\Psi}^{-1}\mathbf{J}_{t\psi}^T\Omega_f\mathbf{w}_{des} \tag{19}$$

Once the desired configuration space velocity vector is obtained, a resolved motion rate approach (Whitney, 1969) is used to obtain the desired configuration and exploit the inverse pose solution.

Next, the controller generates joint-level commands to accomplish the desired tasks. Due to the flexibility of the actuation lines, compensation is required for both achieving the desired pose and applying the desired wrench at the end-effector. Such actuation compensation methods were described in Xu and Simaan (2006) and Simaan et al. (2009). Using the static model proposed in equation (7) and the desired force $\mathbf{w}_{ref}$, the actuation compensation law is obtained as in equation (12).

4.4. Compensation of uncertainties

During control of the real continuum robot there will be a deviation $\boldsymbol{\lambda}$ between the desired actuation force vector $\boldsymbol{\tau}_{des}$ and the sensed actuation force vector $\boldsymbol{\tau}_{curr}$. This deviation is due to friction and extension in the actuation lines, perturbation of the bending shape from the ideal circular configuration, and geometric and static parameters. Thus, the sensed actuation force vectors is as follows

$$\boldsymbol{\tau}_{curr} = \boldsymbol{\tau}_{des} + \boldsymbol{\lambda} \tag{20}$$

In Goldman et al. (2014), the authors showed that the force deviation $\boldsymbol{\lambda}$ is a function of the configurations $\boldsymbol{\Psi}$ of the manipulator and the joint-space velocities $\dot{\mathbf{q}}$. Several methods have been proposed in order to characterize friction and uncertainties. For example, in Mahvash and Okamura (2006), the authors proposed a discrete Dahl model for friction compensation in a master console. In Penning et al. (2011), the authors included a Dahl friction model into the control architecture of steerable catheters. In Lock and Dupont (2011), the authors proposed a method for friction estimation and compensation in concentric tube robots. In Goldman et al. (2014), the authors used a nonlinear regression via support vector regressors to compensate for lumped uncertainties in multi-backbone, multi-segment continuum robots. In this work, we experimentally evaluated uncertainties vector $\boldsymbol{\lambda}$ across the robot's workspace and populated a lookup table for real-time control.

5. Experimental results

The proposed control framework was implemented on the one-segment multi-backbone continuum robot of Figure 3. Three experiments are presented in the reminder of this section: force regulation in the $\hat{\mathbf{x}}_0$- and $\hat{\mathbf{y}}_0$-directions, shape estimation and stiffness characterization. The continuum segment is able to translate along the insertion axis (axis $\hat{\mathbf{z}}_0$ in Figure 1) providing the end-effector with a total of three degree-of-freedom (Dof); q_{ins} and angles θ and δ. Intrinsic

Table 1. Kinematic and static parameters of the continuum robot used in the experiments.

r [mm]	L [mm]	β [°]	d [mm]	E_Y [N/mm^2]	o_d [mm]	I [mm^4]
1.8	17.5	120	13.5	6.5×10^4	0.3	3.9761×10^{-4}

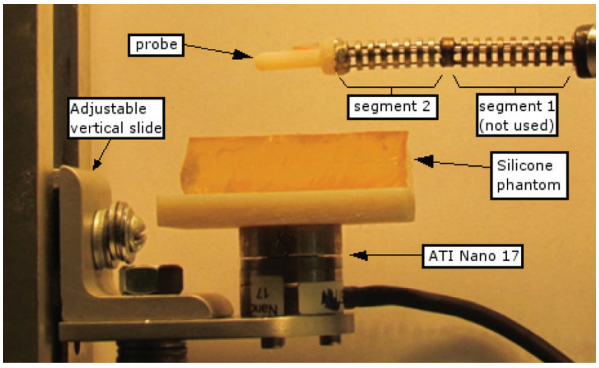

Fig. 3. Experimental setup for force regulation experiments. The setup consist of the continuum manipulator, the ATI Nano force/torque sensor and a hand-controlled linear actuator for the placement of the sensor at different heights.

wrench estimation was implemented according to Appendix B while assuming point contact at the robot tip. Multiple experiments were carried out to validate the efficacy of the proposed framework. While the motion controller always controls motion along the insertion axis direction (the estimation algorithm is not able to sense forces in the $\hat{\mathbf{z}}_0$ -direction (Xu and Simaan, 2008)), the force controller switches between regulating a force in the $\hat{\mathbf{x}}_0$- or $\hat{\mathbf{y}}_0$-directions depending on the task. Table 1 provides the numerical values of the kinematic and static parameters of the robot used for experiments. The radius r is the radial distance from the secondary backbone to the central backbone, L is the nominal length of the continuum segment, β is the division angle between secondary backbones, E_Y is the Young's modulus of the NiTi backbones, o_d is the outer diameter of the backbones and $I = \frac{\pi}{64} o_d{}^4$ is the second area moment of each backbone.

5.1. Estimation of uncertainties

Uncertainties are due to: 1) deviation of the kinematic and static parameters from the nominal ones reported in Table 1; 2) unmodeled friction along the actuation lines; 3) statics and kinematics modeling assumptions; 4) actuation unit assembly. The algorithm presented in Xu and Simaan (2008) was evaluated on a much bigger continuum robot (Ø9 mm) with very short actuation lines in order to minimize modeling and setup uncertainties. The robot used in this work is a Ø5 mm continuum robot with a cone that reroutes the actuation lines and an actuation line length of more than 300 mm. In this work, we calibrate actuation uncertainties by populating a look-up table that depends on the configuration of the continuum manipulator. In this work, we populated one lookup table for each backbone. Each entry in the lookup tables represents $\lambda_i = \tau_{curr_i} - \tau_{des_i}$ for a corresponding backbone i = 1,2,3. The 36 $\times$ 18 were populated for δ and θ increments of 5° for $\delta \in [-90°, 90°]$, $\theta \in [0°, 90°]$. During the experiments the code linearly interpolated the values of the lookup tables.

5.2. Force regulation

This section presents force regulation experimental results. The experiments demonstrate the ability of the controller to regulate a predetermined force in both $\hat{\mathbf{x}}_0$- and $\hat{\mathbf{y}}_0$-directions at different configurations. The experimental setup (Figure 3) consists of a Ø5 mm continuum robot, an interaction probe with a Ø5 mm spherical tip, a delrin block for supporting a silicone phantom and an ATI Nano 17 SI-12-0.12 for ground truth.

In order to test the force estimation and force controller efficacy in the $\hat{\mathbf{x}}_0$-direction the continuum robot was bent to the following three configurations; $\theta = 80°$, $\delta = 0°$, $\theta = 60°$, $\delta = 0°$, and $\theta = 40°$, $\delta = 0°$. At each configuration, a reference force magnitude of 5 gram-force, 10 gram-force and 15 gram-force were commanded. Data from the force estimator and the ATI Nano 17 were compared and the rise time and steady state error computed. Figures 4 to 6 show the step response for force magnitudes 5 gram-force, 10 gram-force and 15 gram-force in the $\hat{x}$-direction at $\theta = 80°$, $\theta = 60°$ and $\theta = 40°$ respectively. Each graph shows the time history of three quantities; desired force (black), sensed force by the ATI Nano 17 (red) and sensed force by the intrinsic force estimator (blue). These results are summarized in Table 2.

Figure 7 shows the step response for a force magnitude of 10 gram-force in the $\hat{\mathbf{y}}_0$-direction at $\theta = 80°$, $\theta = 60°$ and $\theta = 40°$. The results are summarized in Table 3.

The experimental results demonstrate both that the hybrid motion/force control is able to regulate forces of different magnitudes in different directions and that the accuracy depends on the configuration of the manipulator. Steady state error in the $\hat{\mathbf{x}}_0$-direction between the force sensed by the ATI Nano 17 and the intrinsic force estimator is mainly due to residual un-modeled uncertainties as more energy is stored into the system ($\theta = \pi$ /2 zero energy, $\theta = 0$ maximum energy). These uncertainties are due to

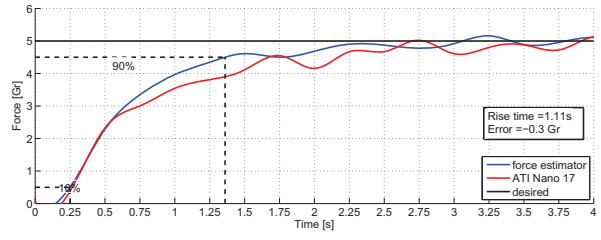

(a) 5 gram-force.

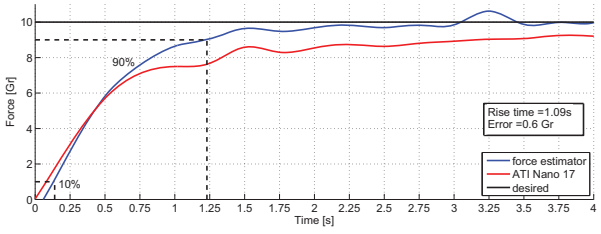

(b) 10 gram-force.

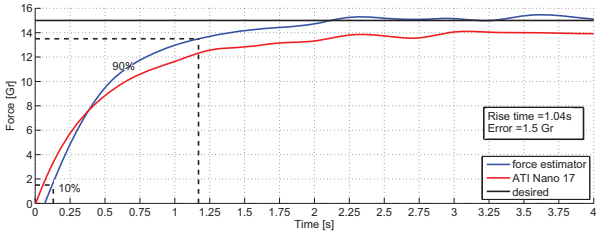

(c) 15 gram-force.

Fig. 4. Force step response on a silicone block in the $\hat{\mathbf{x}}_0$-direction from a starting configuration of $\theta = 80$, $\delta = 0$.

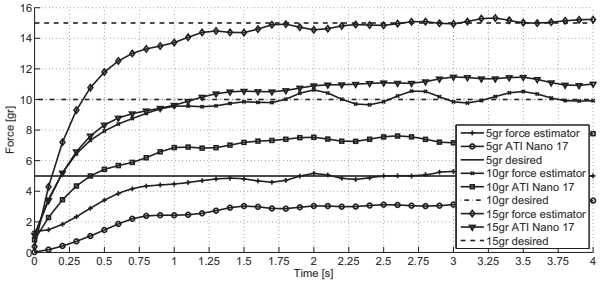

Fig. 5. Force step response on a silicone block in the $\hat{\mathbf{x}}_0$ -direction from a starting configuration of $\theta = 60$, $\delta = 0$.

static and dynamic friction, unpredicted bending shape and extension/contraction of the actuation lines. The high steady state error in the $\hat{\mathbf{y}}_0$-direction (especially when the segment is bent) is due to the low torsional rigidity of the robot. This torsional compliance also limits the sensitivity of the wrench estimation algorithm as already reported in Xu and Simaan (2008). In addition, the look-up tables used in the experiments were not populated using side motions along the δ degree-of-freedom and therefore no friction compensation for those directions was available.

Multimedia Extension 1 in Appendix A demonstrates the tasks of force regulations and hybrid motion/force control under telemanipulation. The end-effector is brought to contact and forces from the extrinsic wrench estimator and

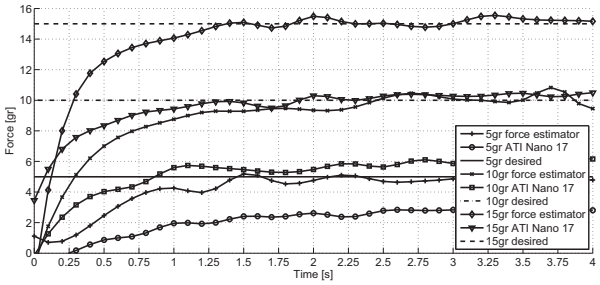

Fig. 6. Force step response on a silicone block in the $\hat{\mathbf{x}}_0$ -direction from a starting configuration of $\theta = 40$, $\delta = 0$.

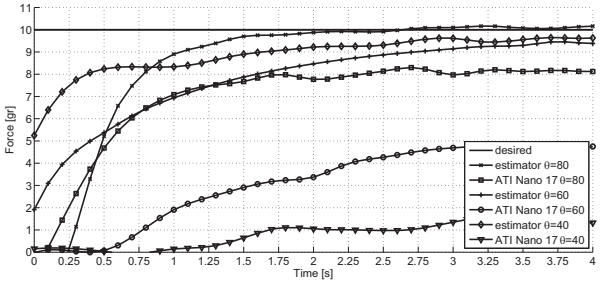

Fig. 7. Force step response on a silicone block in the $\hat{\mathbf{y}}_0$-direction for varying θ and $\delta = 0$.

Table 2. Experimental result of force regulation in the $\hat{x}$ -direction for three configurations $\theta = 80°$, $60°$, $40°$, and three force magnitudes 5 gram-force, 10 gram-force and 15 gram-force.

θ[°]	Force [gram-force]	Rise Time [s]	Steady State Error [gram-force]
80	5	1.11	−0.30
80	10	1.09	0.60
80	15	1.04	1.50
60	5	1.03	1.30
60	10	0.77	3.00
60	15	0.88	3.00
40	5	1.35	1.35
40	10	1.03	4.30
40	15	0.67	4.20

Table 3. Experimental result of force regulation in the $\hat{y}$ -direction for three configurations $\theta = 80°$, $60°$, $40°$, and an applied force of 10 gram-force.

θ[°]	Force [gram-force]	Rise Time [s]	Steady State Error [gram-force]
80	10	0.75	1.90
60	10	2.72	4.10
40	10	1.63	8

the ATI Nano 17 are reported in real-time. Once contact is established, force regulation is enabled and forces in the $\hat{\mathbf{x}}_0$- and $\hat{\mathbf{y}}_0$-direction are regulated while the motion in the $\hat{\mathbf{z}}_0$-direction is controlled by the user.

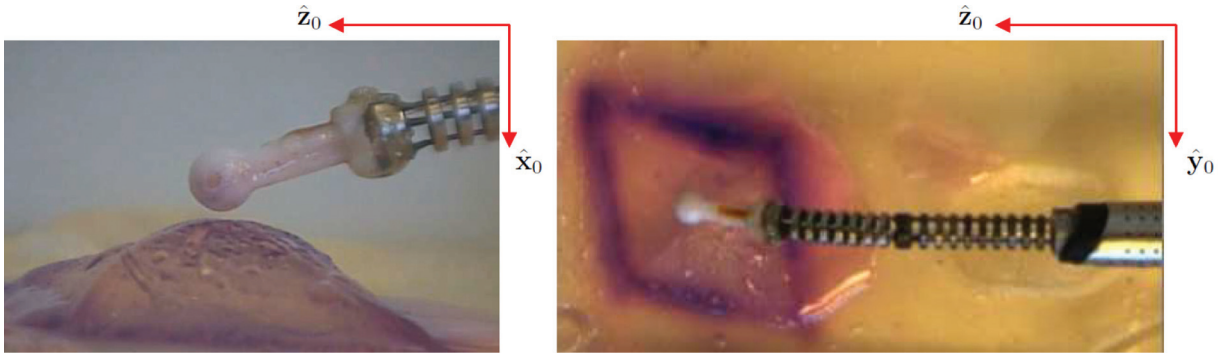

Fig. 8. Experimental setup for shape estimation of a silicon diamond-shaped extrusion. The extrusion plane is placed approximately 18 mm from the origin along the $\hat{\mathbf{x}}_0$-direction. The user actively controlled motion of the probe in the $\hat{\mathbf{y}}_0$- and $\hat{\mathbf{z}}_0$-directions. The force controller regulates a force with a magnitude of 10 gram-force in the $\hat{\mathbf{x}}_0$-direction.

5.3. Force-regulated shape estimation

This section presents the experimental results for shape estimation using force-controlled tele-manipulation. The user is able to control the end-effector while free of contact, and engage the force control in pre-determined directions when in contact with the environment. The experimental setup (Figure 8) consists of a Ø5 mm continuum robot, a diamond-shape silicone phantom, an Ascension Technologies trakSTAR 2 with flat transmitter placed under the phantom and a Force Dimension Omega 7.

The Ø5 mm continuum robot is equipped with a Ø5 mm spherical probe that alleviates sharp interaction with the soft environment. A Ø0.9 mm electro-magnetic coil was delivered through one of the robot's working channels and secured to the probe. The silicone diamond-shaped extrusion is placed in a YZ-plane at a distance of approximately 18 mm from the robot's reference frame as shown in Figure 8. The motion of the end-effector in the $\hat{\mathbf{y}}_0$- and $\hat{\mathbf{z}}_0$-directions were commanded via a Force Dimension Omega 7 with 3-axis force feedback. Position commands were sent over the local area network (LAN) using user datagram protocol (UDP) at 100 Hz. The end-effector's position was acquired at 125 Hz using the Ascension Technology trakSTAR 2 and sent over the LAN using UDP at 100 Hz. The high-level motion and force controllers, and the wrench estimator run at 200 Hz while the low-level joint controller runs at 1 kHz. Switching between full motion control and hybrid motion/force control was enabled using the 7th axis of the Omega 7 (gripper).

The continuum robot, under full motion telemanipulation mode, is guided to reach a point on the silicone phantom. Once hybrid motion/force control is enabled, the robot autonomously regulates a force of 10 gram-force in the $\hat{\mathbf{x}}_0$-direction. Position data of the probe were only collected when the sensed force in the $\hat{\mathbf{x}}_0$-direction was smaller or equal to 5 gram-force and the hybrid motion/force controller was engaged. These conditions ensured that each data point was actually on the surface of the silicon phantom. Switching between full motion/force control and hybrid motion/force control allowed to cover a workspace of 18 mm $\times$ 30 mm $\times$ 40 mm. Ground truth shape data was obtained using a Ø5 mm spherical probe equipped with a Ø0.9 mm magnetic coil. The probe was manually swept over the silicone phantom and data collected. The use of an identical probe equipped with a similar sensor ensures comparison of data having the same accuracy, repeatability, noise and uncertainties. Position data from the electro-magnetic tracker were stored and linearly interpolated using Matlab function *griddata*. This function interpolates the surface at query points on the YZ-plane and returns the interpolated value along the $\hat{\mathbf{x}}_0$-direction. Multiple data points are automatically averaged during the interpolation.

The estimated shape and shape error using the continuum robot with a 10 gram-force regulated telemanipulation scan are shown in Figure 9. A color map (blue to red) identifies different surface heights. As expected, the maximum deviation is found at the boundaries of the robot's workspace along the $\hat{\mathbf{y}}_0$-axis. In fact, in order for the continuum segment to stretch along the $\hat{\mathbf{y}}_0$-axis the bending angle θ decreases considerably and the δ -angle decreases (positive $\hat{\mathbf{y}}_0$) or increases (negative $\hat{\mathbf{y}}_0$). As shown in the force regulation experiments reported in the previous section, the sensitivity of the force estimation in the $\hat{\mathbf{x}}_0$-direction decreases considerably while the sensitivity in the $\hat{\mathbf{y}}_0$-direction increases. Although the controller is unable to regulate the requested amount of force due to the limitations of the intrinsic force estimator, the continuum manipulator maintains contact with the surface. This phenomenon is not seen at the boundaries of the workspace along the $\hat{\mathbf{z}}_0$-direction because the insertion stage provides most of the displacement.

Multimedia Extension 2 in Appendix A shows the complete process of estimating an unknown shape under telemanipulation combined with hybrid motion/force control. The operator is able to switch between full 3-DoF motion control and 2-DoF motion with 1-DoF force control. The probe equipped with the magnetic sensor is read and a 3D map is constructed and shown to the user in real-time.

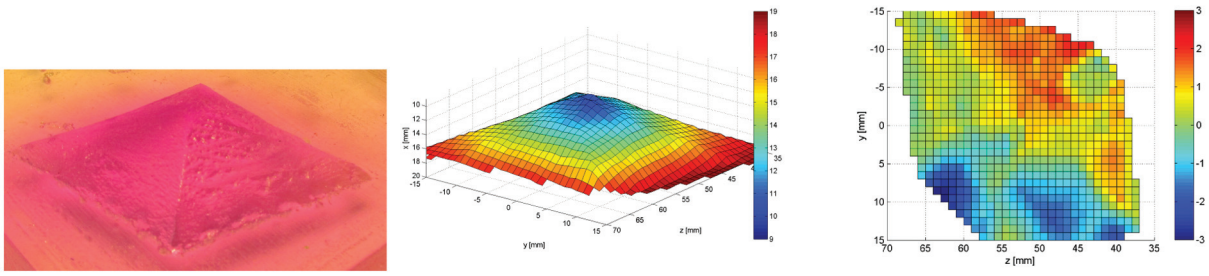

Fig. 9. (a) Real shape, (b) estimated shape, (c) shape error under 10 gram-force force-regulated scan.

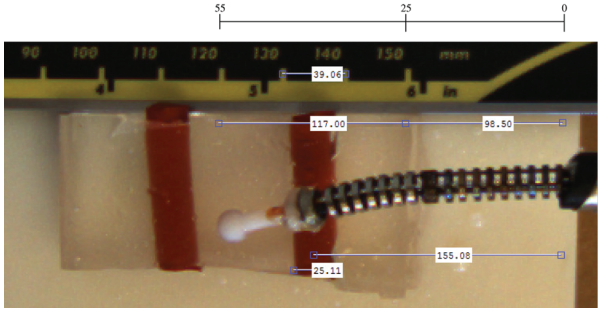

Fig. 10. Setup measurements to localize the mockup blood vessel. The image shows the setup, a ruler and pixel measurements taken with the Matlab Image Processing Toolbox. From the image it is possible to define a scaling factor that relates pixels to mm, the distance of the centerline of the blood vessel from the base of the robot and its width.

5.4. Stiffness imaging

This section presents experimental results on stiffness characterization of soft tissues using the proposed hybrid motion/force controller. The goal of the experiment is to build a relative stiffness image of the surrounding environment using both position and force data. The map identifies changes in stiffness rather than displaying exact real values of tissue stiffness. One way of estimating the change in stiffness is to repetitively scan the surface, applying different force magnitudes and recording the displacement of each point between scans. The experimental setup (Figure 10) consists of a Ø5 mm continuum robot, a plastic probe with a Ø5 mm spherical tip, a Ø0.9 mm electromagnetic sensor and a silicone phantom with an embedded rubber tube. The embedded tube is stiffer than the silicone phantom and locally increases the stiffness of the whole sample.

Two consecutive surface scans were completed under hybrid motion/force control applying respectively 5 and 25 gram-force. The first scan is used to estimate the unknown shape by minimizing deflection while ensuring contact. The latter is used to evaluate deflection under a known load. The force magnitude used in the second scan depends on the stiffness of the surface, accuracy and the signal-to-noise ratio of the measurement system used. In this particular case it was found that a 25 gram-force produced enough deflection to be observed by the Ascension trakSTAR 2. After selecting the desired force magnitude, the operator guides the robot to cover the designated area (Figure 10). The rubber tube is embedded at approximately 155 pixels (px) from the base of the robot. Using the ruler shown in Figure 10, it is possible to define a scaling factor between image pixels and mm. In this case, 39 px = 10 mm. Using this ratio, the position of the rubber tube is identified at approximately 39.7 mm from the base of the manipulator. The flexible manipulator was used to scan a rectangular area of approximately 20 × 30 mm. Position data during each scan were recorded from the electro-magnetic sensor placed at the tip along with the sensed force in the $\hat{\mathbf{x}}_0$-direction and smoothed by spline interpolation. The estimated surfaces under 5 gram-force and 25 gram-force force control are shown in Figure 11.

In order to characterize the difference in stiffness along the surface (not the absolute stiffness) a linear spring-model is used. Figure 12(a) shows the estimated stiffness values across the scanned area while Figure 12(b) shows the XZ-plane cross-section of both surface scans. The contour map shows a peak of 0.3 N/mm at approximately 40 mm from the base of the robot. The estimated stiffness decreases to 0.25 N/mm, 0.2 N/mm and 0.15 N/mm respectively along both positive and negative $\hat{\mathbf{z}}_0$-directions. Lower stiffness is estimated at the boundaries of the scanned surface (z = 55 and z = 25). This result agrees with the impingement comparison shown in 12(b) and Figure 10 that shows the rubber tube laying along the $\hat{\mathbf{y}}_0$-axis at approximately 155 px = 39.7 mm from the base of the robot.

6. Conclusions

In this paper, an adaptation of the classic hybrid motion/force controller for continuum robots is presented and evaluated. The dual control inputs (force and motion) are merged in the configuration space of the manipulator using both differential inverse kinematics (motion) and the configuration space compliance matrix (force). By producing consistent configuration space commands, the inverse

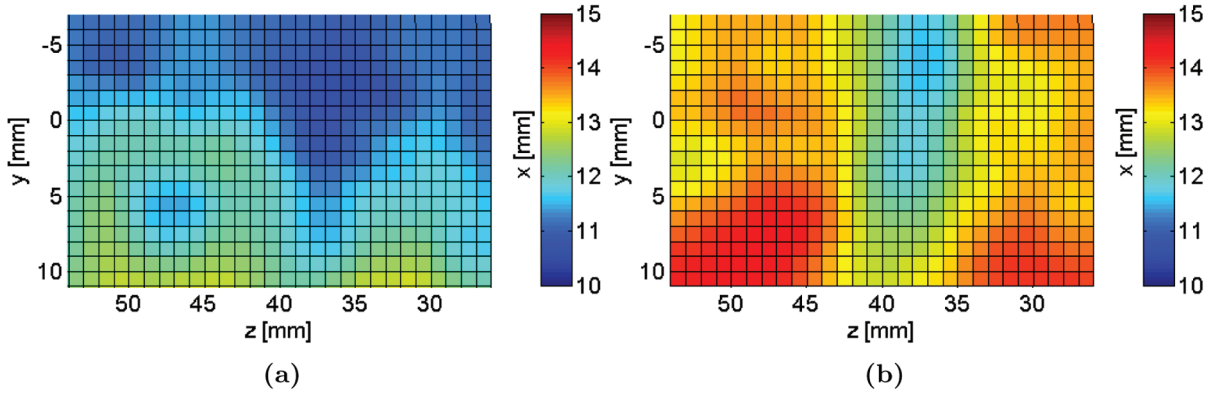

Fig. 11. (a) Colormap of the estimated surface applying 5 gram-force, (b) Colormap of the estimated surface applying 25 gram-force.

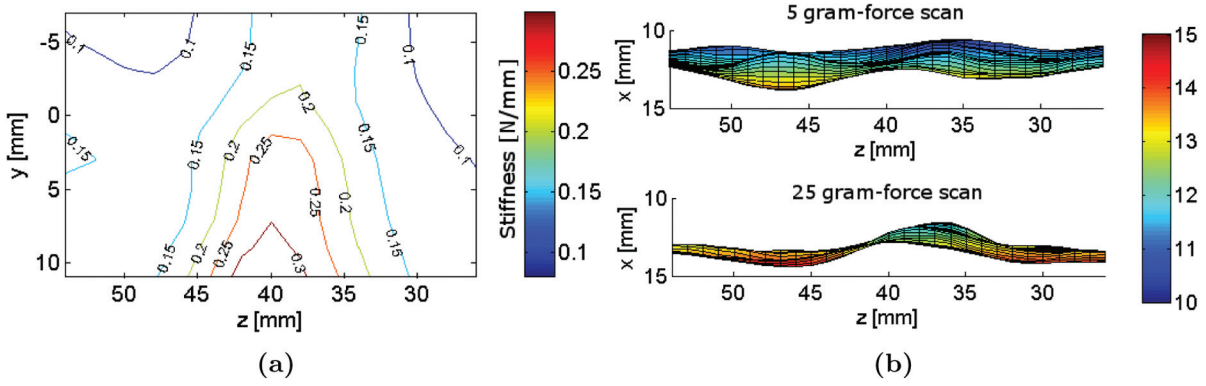

Fig. 12. (a) Contour map of the estimated stiffness, (b) XZ-plane cross section of the two scans used to estimate the stiffness.

position of the manipulator is used along with model-based actuation compensation methods and feed-forward force-inputs. The framework was evaluated on a single-segment continuum robot suitable for natural orifice translumenal endoscopic surgery. Firstly, experiments demonstrated the ability to estimate and regulate forces at the tip of the robot. The controller's performances are tied to the intrinsic force estimator's sensitivity and accuracy. Secondly, force-regulated shape estimation of unknown flexible environments was demonstrated. The force controller ensured that the probe maintained contact with the tissue phantom. Finally, force-regulated stiffness estimation of unknown flexible environments was conducted. Force and position data from subsequent scans with different forces were compared and a linear stiffness model was used to produce a stiffness image of the explored workspace. The experiments demonstrated that this strategy allows discernment of change in stiffness. The framework proposed in this work makes the first step toward improving situation awareness, estimation and mapping in challenging environments such as minimally invasive robotic surgery. The proposed algorithm was already used in a proof of concept of simultaneous localization and mapping of body organs (BodySLAM) (Sanan et al., 2014) by providing simultaneous shape and stiffness information of soft environments. Future work will demonstrate the proposed framework on multi-segment continuum robots and provide efficient and precise algorithms for shape estimation and stiffness imaging (Goldman et al., 2012) in deep surgical sites.

Funding

This work was supported by the National Science Foundation (NSF) (grant number IIS-1063750) and in part by grant number IIS -1327566.

Note

1. Here we adopt the notation of axis coordinates for motion screws $(T = [\mathbf{v}_0^T, \boldsymbol{\omega}^T]^T)$ where $\mathbf{v}_0$ is the linear velocity and $\boldsymbol{\omega}$ is the angular velocity. We also adopt the ray coordinate representation for wrenches $(F = [\mathbf{f}^T, \mathbf{m}^T]^T)$ where $\mathbf{f}$ is a force vector and $\mathbf{M}$ is a moment.

References

Agrawal V, Peine WJ, Yao B and Choi S (2010) Control of cable actuated devices using smooth backlash inverse. In: *2010 IEEE international conference on robotics and automation*, Anchorage, USA, pp. 1074–1079.

Bajo A, Goldman RE and Simaan N (2011) Configuration and joint feedback for enhanced performance of multi-segment continuum robots. In: *2011 IEEE international conference on robotics and automation*, Shanghai, China. Shanghai: IEEE.

Bajo A and Simaan N (2010) Finding lost wrenches: Using continuum robots for contact detection and estimation of contact location. In: *2010 IEEE international conference on robotics and automation*, Anchorage, USA.

Bajo A and Simaan N (2012) Kinematics-based detection and localization of contacts along multisegment continuum robots. *IEEE Transactions on Robotics* 28(2): 291–302.

Baki P, Szekely G and Kosa G (2012) Miniature tri-axial force sensor for feedback in minimally invasive surgery. In: *2012 4th IEEE RAS & EMBS international conference on biomedical robotics and biomechatronics (BioRob)*, Roma, Italy, pp. 805–810. Roma: IEEE.

Basilevsky A (1983) *Applied Matrix Algebra in the Statistical Sciences*. Mineola: Dover Publications.

Braganza D, Dawson D, Walker I and Nath N (2007) A neural network controller for continuum robots. *IEEE Transactions on Robotics* 23(6): 1270–1277.

Camarillo DB, Carlson CR and Salisbury JK (2009) Configuration tracking for continuum manipulators with coupled tendon drive. *IEEE Transactions on Robotics* 25(4): 798–808.

Camarillo DB, Milne CF, Carlson CR, Zinn MR and Salisbury JK (2008) Mechanics modeling of tendon-driven continuum manipulators. *IEEE Transaction on Robotics* 24(6): 1262–1273.

Chirikjian G (1993) General methods for computing hyper-redundant manipulator inverse kinematics. In: *Proceedings of 1993 IEEE/RSJ international conference on intelligent robots and systems (IROS'93)*, volume 2, Yokohama, Japan, pp. 1067–1073. Yokohama: IEEE.

Chirikjian GS and Burdick JW (1994) A modal approach to hyper-redundant manipulator kinematics. *IEEE Transaction on Robotics and Automation* 10(3): 343–354.

Croom JM, Rucker DC, Romano JM and Webster RJI (2010) Visual sensing of continuum robot shape using self-organizing maps. In: *2010 IEEE international conference on robotics and automation*, Anchorage, USA, pp. 4591–4596.

Featherstone R (2004) Modeling and control of contact between constrained rigid bodies. *IEEE Transaction on Robotics and Automation* 20(1): 82–92.

Goldman RE, Bajo A, MacLachlan LS, Pickens R, Herrell SD and Simaan N (2013) Design and performance evaluation of a minimally invasive telerobotic platform for transurethral surveillance and intervention. *IEEE transactions on bio-medical engineering* 60(4): 918–25.

Goldman RE, Bajo A and Simaan N (2011) Compliant motion control for continuum robots with intrinsic actuation sensing. In: *2011 IEEE international conference on robotics and automation*.

Goldman RE, Bajo A and Simaan N (2012) Algorithms for autonomous exploration and estimation in compliant environments. *Robotica* 31(1): 71–87.

Goldman RE, Bajo A and Simaan N (2014) Compliant motion control for multisegment continuum robots with actuation force sensing. *IEEE Transactions on Robotics* 30(4): 890–902.

Gravagne IA, Rahn CD and Walker ID (2003) Large deflection dynamics and control for planar continuum robots. *IEEE/ASME Transaction on Mechatronics* 8(2): 299–307.

Gravagne IA and Walker ID (2000) Kinematic transformations for remotely-actuated planar continuum robots. In: *2000 IEEE international conference on robotics and automation*, San Francisco, USA, April, pp. 19–26.

Hannan MW and Walker ID (2003) Kinematics and the implementation of an elephant' s trunk manipulator and other continuum style robots. *Journal of Robotic Systems* 20(2): 45–63.

Hogan N (1985) Impedance control: An approach to manipulation: Part I – Theory. *Journal of Dynamic Systems, Measurement, and Control* 107(1): 1.

Ivanescu M and Stoian V (1995) A variable structure controller for a tentacle manipulator. In: *Proceedings of 1995 IEEE international conference on robotics and automation*, volume 3, Nagoya, Japan, pp. 3155–3160. Nagoya: IEEE.

Jones BA and Walker ID (2006) Kinematics for multisection continuum robots. *IEEE Transactions on Robotics* 22(1): 43–57.

Kapadia AD, Fry KE and Walker ID (2014) Empirical investigation of closed-loop control of extensible continuum manipulators. In: *2014 IEEE/RSJ international conference on intelligent robots and systems*, pp. 329–335. IEEE.

Kesner SB and Howe RD (2011) Force control of flexible catheter robots for beating heart surgery. In: *2011 IEEE international conference on robotics and automation*, Shanghai, China, pp. 1589–1594.

Kesner SB, Howe RD and Member S (2011) Position control of motion compensation cardiac catheters. *IEEE Transaction on Robotics* 27(6): 1045–1055.

Khatib O (1987) A unified approach for motion and force control of robot manipulators: The operational space formulation. *IEEE Journal of Robotics and Automation* 3(1): 43–53.

Lipkin H and Duffy J (1988) Hybrid twist and wrench control for a robotic manipulator. *Transaction of the ASME* 110: 138–144.

Lock J and Dupont PE (2011) Friction modeling in concentric tube robots. In: *2011 IEEE international conference on robotics and automation*, Shanghai, China, pp. 1139–1146.

Mahvash M and Dupont PE (2010) Mechanics of dynamic needle insertion into a biological material. *IEEE transactions on biomedical engineering* 57(4): 934–43.

Mahvash M and Dupont PE (2011) Stiffness control of surgical continuum manipulators. *IEEE Transaction on Robotics* 27(2): 334–345.

Mahvash M and Okamura AM (2006) Friction compensation for a force-feedback telerobotic system. In: *2006 IEEE international conference on robotics and automation*, Orlando, USA.

Mason M and Salisbury K (1985) *Robot Hands and the Mechanics of Manipulation*. Cambridge, MA: MIT Press.

Mason MT (1981) Compliance and force control for computer controlled manipulators. *IEEE Transaction on Systems, Man, and Cybernetics* 11(6): 418–432.

Penning RS, Jung J, Borgstadt JA, Ferrier NJ and Michael R (2011) Towards closed loop control of a continuum robotic manipulator for medical applications. In: *2011 IEEE international conference on robotics and automation*, Shanghai, China, pp. 4822–4827.

Piltan F and Tayebi Haghighi S (2012) Design gradient descent optimal sliding mode control of continuum robots. *IAES International Journal of Robotics and Automation (IJRA)* 1(4): 175–189.

Raibert MH and Craig JJ (1981) Hybrid position/force control of manipulators. *ASME Journal of Dynamic Systems Measurement Control* 102: 126–133.

Robinson G and Davies J (1999) Continuum robots - a state of the art. In: *1999 IEEE International conference on robotics and automation*, volume 4, Detroit, USA, pp. 2849–2854. Denver: IEEE.

Rucker DC and Webster III RJ (2011) Deflection-based force sensing for continuum robots: A probabilistic approach. In: *2011*

IEEE/RSJ international conference on intelligent robots and systems, pp. 3764–3769.

Salisbury J (1980) Active stiffness control of a manipulator in cartesian coordinates. In: *1980 19th IEEE conference on decision and control including the symposium on adaptive processes*, pp. 95–100.

Sanan S, Tully S, Bajo A, Simaan N and Choset H (2014) Simultaneous compliance and registration estimation for robotic surgery. In: *Robotics science and systems*, Berkeley, USA, 12–16 July.

Seibold U, Kübler B and Hirzinger G (2005) Prototype of instrument for minimally invasive surgery with 6-axis force sensing capability. In: *IEEE international conference on robotics and automation*, Barcelona, Spain, pp. 498–503.

Simaan N, Xu K, Wei W, Kapoor A, Kazanzides P, Taylor RH and Flint P (2009) Design and integration of a telerobotic system for minimally invasive surgery of the throat. *The International Journal of Robotics Research* 28(9): 1134–1153.

Trivedi D and Rahn CD (2014) Model-based shape estimation for soft robotic manipulators: The planar case. *Journal of Mechanisms and Robotics* 6(2): 021005.

Tully S, Bajo A, Kantor G, Choset H and Simaan N (2012) Constrained filtering with contact detection data for the localization and registration of continuum robots in flexible environments. In: *2012 IEEE international conference on robotics and automation*, St. Paul, USA.

Valdastri P, Harada K, Menciassi A, Beccai L, Stefanini C, Fujie M and Dario P (2006) Integration of a miniaturised triaxial force sensor in a minimally invasive surgical tool. *IEEE transactions on bio-medical engineering* 53(11): 2397–2400.

Webster III RJ and Jones BA (2010) Design and kinematic modeling of constant curvature continuum robots: A review. *The International Journal of Robotics Research* 29(13): 1661–1683.

Wei W and Simaan N (2012) Modeling, force sensing, and control of flexible cannulas for microstent delivery. *Journal of Dynamic Systems, Measurement, and Control* 134(4): 041004.

Whitney DE (1969) Resolved motion rate control of manipulators and human prostheses. *IEEE Transactions on Man-Machine Systems* 10(2): 47–53.

Whitney DE (1977) Force feedback control of manipulator fine motions. *Journal of Dynamic Systems, Measurement, and Control* 99(2): 91.

Xu K and Simaan N (2006) Actuation compensation for flexible surgical snake-like robots with redundant remote actuation. In: *2006 IEEE international conference on robotics and automation*, Orlando, USA, May, pp. 4148–4154.

Xu K and Simaan N (2008) An investigation of the intrinsic force sensing capabilities of continuum robots. *IEEE Transactions on Robotics* 24(3): 576–587.

Xu K and Simaan N (2010a) Analytic formulation for kinematics, statics, and shape restoration of multibackbone continuum robots via elliptic integrals. *ASME Journal of Mechanisms and Robotics* 2(1): 011006–011006–13.

Xu K and Simaan N (2010b) Intrinsic wrench estimation and its performance index for multisegment continuum robots. *IEEE Transactions on Robotics* 26(3): 555–561.

Yoshikawa T (2000) Force control of robot manipulators. In: *2000 IEEE international conference on robotics and automation*, San Francisco, USA, April, pp. 220–226.

Zanganeh KE and Angeles J (1995) The inverse kinematics of hyper-redundant manipulators using splines. In: *1995 IEEE international conference on robotics and automation*, Nagoya, Japan.

Appendix A: Index to Multimedia Extensions

Archives of IJRR multimedia extensions published prior to 2014 can be found at http://www.ijrr.org, after 2014 all videos are available on the IJRR YouTube channel at http://www.youtube.com/user/ijrrmultimedia

Table of Multimedia Extensions

Extension	Media type	Description
1	Video	Hybrid motion/force control
2	Video	Real-time shape estimation under telemanipulation control

Appendix B: Intrinsic wrench estimation

Continuum robots with actuation force sensing allow to estimate external wrenches acting at the tip. These capabilities are investigated in Xu and Simaan (2008) where the authors presented a minimization algorithm for estimating forces with a single segment and presented the full estimation in Xu and Simaan (2010b). For completeness, this appendix summarizes the results from Xu and Simaan (2008, 2010b) while assuming point contact at the tip of the robot. Using the statics model in equation (7), the external wrench acting at the tip of the continuum robot is given by

$$\mathbf{w}_{curr} = \left(\mathbf{J}_{t\psi}^T\right)^{\dagger}\left(\nabla \mathbf{U} - \mathbf{J}_{q\psi}^T(\tau_{curr} - \lambda)\right) + \left(\mathbf{I} - \left(\mathbf{J}_{t\psi}^T\right)^{\dagger}\mathbf{J}_{t\psi}^T\right)\eta \tag{21}$$

where

$$\eta = \mathbf{D}^{\dagger}\mathbf{F}^T\mathbf{S}_e\left(\mathbf{w}_{se} - \left(\mathbf{J}_{t\psi}^T\right)^{\dagger}\left(\nabla \mathbf{U} - \mathbf{J}_{q\psi}^T(\tau_{curr} - \lambda)\right)\right) \tag{22}$$

$$\mathbf{D} = \left(\mathbf{I} - \left(\mathbf{J}_{t\psi}^T\right)^{\dagger}\mathbf{J}_{t\psi}^T\right)^T\mathbf{S}_e\left(\mathbf{I} - \left(\mathbf{J}_{t\psi}^T\right)^{\dagger}\mathbf{J}_{t\psi}^T\right) \tag{23}$$

$$\mathbf{F} = \left(\mathbf{I} - \left(\mathbf{J}_{t\psi}^T\right)^{\dagger}\mathbf{J}_{t\psi}^T\right) \tag{24}$$

$$\mathbf{S}_e = \begin{bmatrix} (\hat{\mathbf{n}}_t \times \hat{\mathbf{n}}_n)(\hat{\mathbf{n}}_t \times \hat{\mathbf{n}}_n)^T & \mathbf{0}_{3\times 3} \\ \mathbf{0}_{3\times 3} & \mathbf{I}_{3\times 3} \end{bmatrix} \tag{25}$$

$$\mathbf{W}_{se} = \begin{bmatrix} c_t\hat{\mathbf{n}}_t + n_t\hat{\mathbf{n}}_n \\ \mathbf{0}_{3\times 1} \end{bmatrix} \tag{26}$$

$\mathbf{S}_e$ and $\mathbf{W}_{se}$ contain a priori knowledge of the contact constraint and guide the estimation algorithm. The a priori knowledge is defined by contact normal vector $\hat{\mathbf{n}}_n$ and contact tangential vector $\hat{\mathbf{n}}_t$. These two vectors define the plane in which the sensable component of the external wrench lies.